Genome stability-related lncRNA ZFPM2-AS1 promotes tumor progression via miR-3065-5p/XRCC4 in hepatocellular carcinoma

JIE LIU[1,2*], HAO ZHANG[1,2*], PENG XIA[1,2], YIMIN ZHU[1,2], KEQUAN XU[1,2], ZHISU LIU[1,2] and YUFENG YUAN[1,2]

[1]Department of Hepatobiliary and Pancreatic Surgery, Zhongnan Hospital of Wuhan University;
[2]Clinical Medicine Research Center for Minimally Invasive Procedure of Hepatobiliary and
Pancreatic Diseases of Hubei Province, Wuhan, Hubei 430071, P.R. China

Abstract. Long noncoding RNAs (lncRNAs) have a certain link to genomic stability (GS). However, the regulatory relationship of lncRNAs and GS has not been thoroughly investigated in hepatocellular carcinoma (HCC). In the present study, samples were retrieved from The Cancer Genome Atlas with somatic mutations and lncRNA expression data. Cox regression analysis was used to identify independent prognostic factors. The RNA levels were determined by reverse transcription-quantitative PCR and protein levels were detected by western blot analysis. Cell Counting Kit-8 and colony-formation assays were used to assess cell viability. Cell migration was measured by wound-healing and Transwell assays. Cell apoptosis and cell-cycle progression were evaluated by flow cytometry. GS was detected by alkaline comet and chromosomal aberration assays. A xenograft model and lung metastasis model were used to assess the role of zinc finger protein, FOG family member 2 antisense 1 (ZFPM2-AS1) in tumor growth *in vivo*. The molecular mechanisms underlying the biological functions of ZFPM2-AS1 were investigated through bioinformatics prediction, RNA pull-down and luciferase reporter assays. A total of 85 genomic instability-related lncRNAs were identified and a prognostic model was developed. The prognostic model exhibited good predictive power (area under the receiver operating characteristic curve, 0.786). ZFPM2-AS1 was significantly upregulated in tumor tissues (P<0.001) and it promoted DNA damage repair (P<0.01) and tumor progression *in vitro* and *in vivo*.

Luciferase reporter assays demonstrated that miR-3065-5p was able to bind directly with ZFPM2-AS1 and X-ray repair cross complementing 4 (XRCC4). ZFPM2-AS1 upregulated XRCC4 expression by acting as a sponge (P<0.001). In the present study, a prognostic model for HCC was developed and validated, and one lncRNA of its components was experimentally investigated. ZFPM2-AS1 regulates XRCC4 by sponging miR-3065-5p to promote GS and HCC progression.

Introduction

Liver cancer is the sixth most common cancer type and the fourth leading cause of death due to cancer globally (1). The carcinogenesis of the liver involves multiple mechanisms, such as immune escape, somatic mutations, abnormal lipid metabolism and aberrant changes in multiple molecular pathways (2,3). It is well known that long noncoding RNAs (lncRNAs) have a critical role in gene regulation (4). However, only limited studies have investigated the regulatory roles of lncRNAs and genomic stability (GS). Multiple lncRNAs have been reported to be abnormally expressed and contribute to malignant phenotypes in hepatocellular carcinoma (HCC). They commonly exert their effects by interacting with DNA, RNA or proteins, or encoding short peptides. For instance, lncRNA proliferating cell nuclear antigen pseudogene 1 promotes hepatitis B virus replication and hepatocarcinogenesis by modulating signalling (5). LncRNA small nucleolar RNA host gene 6 accelerates the development of HCC by interacting with heterogeneous nuclear ribonucleoprotein L/polypyrimidine tract binding protein 1 to facilitate the destabilisation of SET domain containing 7/leucine zipper transcription factor like 1 mRNA (6). Significant upregulation of HOX transcript antisense RNA expression in HCC is associated with poor prognosis (7). Apart from that, lncRNAs affect the development of cancer by influencing tumor metabolism and immunomodulation. Hepatocellular carcinoma upregulated long non-coding RNA enhances glycolysis and promotes the proliferation of liver cancer cells through lactate dehydrogenase A and pyruvate kinase M1/2 (8). LncRNAs may regulate tumor immunity by directly influencing immune-associated genes (9). Aberrant expression of lncRNAs is involved in various biological processes of cancers. The competing endogenous RNA (ceRNA) mechanism is one of the most

Correspondence to: Professor Zhisu Liu or Professor Yufeng Yuan, Department of Hepatobiliary and Pancreatic Surgery, Zhongnan Hospital of Wuhan University, 169 Donghu Road, Wuhan, Hubei 430071, P.R. China
E-mail: liuzs53@sina.com
E-mail: yuanyf1971@whu.edu.cn

*Contributed equally

well-studied aspects of lncRNA mechanisms. LncRNAs is able to interact with microRNAs (miRNAs) and inhibit gene silencing caused by miRNAs (10). By modulating focal adhesion signaling, ITGB8-AS1 acts as a ceRNA to regulate cell proliferation and tumor formation (11).

Increasing evidence suggests that GS is inextricably linked to cancer (12). GS appears to influence the multistep process of cancer progression through abnormal DNA repair pathways and dysregulation of genes encoding homologous recombination proteins (13). Aberrant lncRNAs have an equally significant impact on GS by regulating key homologous recombination DNA repair genes, which in turn influences tumorigenesis (14). DNA double-strand break repair is regulated by lncRNA lnc-RI by stabilising RAD51 Recombinase (RAD51) as a ceRNA (15). The non-coding RNA activated by DNA damage forms a topoisomerase complex that is essential for GS (16). Noncoding RNA activated by DNA damage regulates GS through Pumilio protein binding (17). The accumulation of mutations in somatic cells is linked to GS and development (18). These studies offer a good basis for the development of a novel carcinogenic mechanism and potential therapeutic targets for HCC via lncRNAs and GS.

Therefore, the present study established a prognostic model related to genomic instability (GI). To verify the relationship between prognostic lncRNAs and GS, the role of the lncRNA zinc finger protein, FOG family member 2 antisense 1 (ZFPM2-AS1) in HCC was investigated through basic experiments.

Materials and methods

Data collection. Data on somatic mutation profiles, RNA expression profiles and clinical characteristics of patients with HCC were obtained from The Cancer Genome Atlas (TCGA) database (https://portal.gdc.cancer.gov/). Samples with missing information on lncRNA and mRNA expression profiles, clinical characteristics or somatic mutations were excluded. A total of 343 patients with HCC were enrolled. Table SI lists all of the websites that were accessed for the present study. Somatic mutations were analyzed and counted by using the 'maftools' R package (v2.10.5) to obtain the tumor mutation burden of each patient. Heatmaps, boxplot graphs, receiver operating characteristic (ROC) analysis with area under the curve (AUC) and Kaplan-Meier survival curves were generated in R (v3.5.2). The GSE14520 (19) and GSE76427 (20) datasets were downloaded from the Gene Expression Omnibus (GEO) database (https://www.ncbi.nlm.nih.gov/geo/). miRDB (http://www.mirdb.org/), LncBase (http://carolina.imis. athena-innovation.gr/diana_tools/web/) and TargetScan (http://www.targetscan.org/vert_72/) were applied to predict candidate binding miRNAs.

Exploration of GI-related lncRNAs. After computing the cumulative number of somatic mutations per patient and then ranking the patients in decreasing order, the top 25% (n=93) and bottom 25% (n=90) were designated as the GI and the GS group, respectively. The 'LIMMA' R package (v3.38.3) was used to compare the lncRNA expression profiles of the two groups of patients. A total of 85 significantly differentially expressed lncRNAs were screened based on the cutoff criteria of fold change >2 and P<0.05. These 85 lncRNAs were defined as GI-related lncRNAs.

Tissue samples and cell culture. Tumor and adjacent nontumor tissues from 80 patients with HCC (age range, 15-91 years; females/males, 4:6) were obtained from Zhongnan Hospital of Wuhan University (Wuhan, China) and collected by surgery. Tissue collection dates ranged from April 2014 to May 2020. The exclusion criteria were patients with a history of local or systemic treatment for HCC or other clinical disorders. None of the patients in this study received any chemotherapy or radiation therapy prior to surgery. All patients provided written informed consent. The present study conformed to the Declaration of Helsinki. The tissue samples were collected with the approval of the ethics committee of Zhongnan Hospital (Wuhan, China; no. KELUN2020100).

Furthermore, five liver cancer cell lines and a normal liver cell line were used: HepG2, Li-7, HCC-LM3, Huh-7, Hep3B and THLE-3. HepG2 is a human liver cancer cell line. All cell lines were maintained in Dulbecco's modified Eagle's medium (DMEM) or minimum essential medium (MEM) containing 10% foetal bovine serum (FBS, Gibco; Thermo Fisher Scientific, Inc.). The cell lines were obtained from the Cell Resource Center of Shanghai Institutes for Biological Sciences, Chinese Academy of Sciences and cultured in a humidified incubator (5% CO_2, 37˚C). All cell lines were authenticated using short tandem repeat profiling.

DNA damage analysis. To detect DNA damage, an alkaline comet assay was performed using a reagent kit (ELK Biotechnology) according to the manufacturer's protocol. ImageJ-OpenComet software [ImageJ, v1.53e; National Institutes of Health (NIH)] was employed to evaluate the results of the comet assay. The extent of DNA damage was expressed as the tail moment, which corresponded to the fraction of the DNA in the tail of the comet.

RNA extraction and reverse transcription quantitative polymerase chain reaction (RT-qPCR) analysis. Total RNA was extracted using the TRIzol method according to the manufacturer's instructions (Vazyme Biotech Co., Ltd.). RT was performed by using an RT kit (cat. no. R223-01; Vazyme Biotech Co., Ltd.). According to the manufacturer's protocol, the reverse transcription conditions were as follows: 42˚C for 2 min, 50˚C for 15 min and 85˚C for 5 sec. The product was used for qPCR. A standard SYBR Green PCR kit (cat. no. Q711-02; Vazyme Biotech Co., Ltd.) was employed to perform qPCR as described previously (21). GAPDH served as an endogenous control. Relative expression was calculated using the comparative quantification cycle (Cq) method ($2^{-\Delta\Delta Cq}$) (22). The thermocycling conditions are provided in Table SII and the primers in Table SIII.

Plasmid, microRNA and short hairpin RNA (shRNA) transfection. For transfection, HCC cells were seeded in T25 flasks one night prior to transfection. When the cell confluence reached 80%, the cells were transfected with ZFPM2-AS1 overexpression plasmid and a corresponding empty plasmid using Lipofectamine 3000 (Thermo Fisher Scientific, Inc.). According to the manufacturer's protocol, 5 μg plasmid, 10 μl

P3000, 10 µl Lipofectamin® 3000 and 500 µl Opti-MEM Medium (Gibco; Thermo Fisher Scientific, Inc.) were mixed gently and then incubated at room temperature (RT) for 15 min. The mixture was then slowly added to HCC cells. After incubating at 37°C for 12 h, the culture medium was subsequently replaced with fresh DMEM supplemented with 10% FBS. HCC cells were harvested at 48 h after plasmid transfection. Total RNA was extracted and used to assess the transfection efficiency via RT-qPCR. ZFPM2-AS1-wild-type (WT)/mutant (MUT) plasmids and X-ray repair cross complementing 4 (XRCC4)-WT/MUT plasmids were constructed by Genomeditech. The seed sequences of ZFPM2-AS1 plasmids were TTTGTTG (WT) and CGGACCT (MUT). The seed sequences of XRCC4 plasmids were TTTGTTG (WT) and CGGACCT (MUT). shRNA, miR-3065-5p primers and miRNA mimic/inhibitor were designed by Wuhan Qingke Biotechnology Co., Ltd. HCC-LM3 and Huh7 cells were transfected with shRNA lentiviral plasmid (pLKO.1-purp). Puromycin (2 µg/ml) was used for sorting positive shRNA cells. TSnanofect (Wuhan Qingke Biotechnology Co., Ltd) was used for transfection of miR-3065-5p mimic/inhibitor. The shRNA and miRNA sequences are presented in Table SIII.

Western blot (WB) analysis. WB was performed using standard methods as described previously (23). The adherent cells were washed twice with cold PBS, trypsinized to collect the cell precipitate and resuspended in PBS. The cell suspension was then centrifuged at 4°C and 500 x g for 3 min and the cell precipitate was harvested. Cells were lysed for 15 min on ice in RIPA buffer (Beyotime Institute of Biotechnology). Cell lysates were centrifuged at 14,000 x g at 4°C for 10 min to collect the supernatant. Protein samples (supernatant) were denatured at 95°C for 10 min. Quantification of protein levels was performed using a BCA kit (Beyotime Institute of Biotechnology). A total of 50 µg protein was loaded per lane and separated by 10% SDS-PAGE and transferred to 0.45-µm polyvinylidene difluoride (PVDF) membranes (Immobilon-P; Millipore) by electro-transblotting, at 300 mA for 1 h. Electro-transblotting was performed by using transblotting buffer (192 mM glycine, 25 mM TrisBase, 20% methanol). Subsequently, 5% skimmed milk was used to block PVDF membranes for 1 h at RT. The membranes were incubated with primary antibodies overnight at 4°C. They were then washed thrice with tris-buffered saline/Tween 20 (TBST) for 30 min and incubated with secondary antibody for 1 h at RT. Finally, the membranes were washed thrice with TBST for 30 min. The antibodies and antibody dilution ratios used in this experiment are listed in Table SIV. Protein expression was identified using enhanced chemiluminescence western blotting detection reagents (Thermo Fisher Scientific, Inc.) and a Tanon-5200 Chemiluminescent Imaging System (Tanon Science & Technology) and densitometrically quantified using Image Lab software (v5.2; BioRad Laboratories, Inc.). GAPDH served as a loading control for normalization.

In vivo experiments. Male mice (BALB/c nude mice; age, 5 weeks; body weight, 18-20 g; Shulaibao Biotech) were housed at 5 per cage under specific pathogen-free conditions (temperature, $21\pm2°C$; humidity, 40-60%; 12-h light/dark cycle; free access to standard sterile food and water) and ear-notched

for identification. For establishing the subcutaneous xenograft model in 10 mice, negative control or HCC-LM3 cells with stable ZFPM2-AS1 knockdown (0.1 ml; $2x10^6$ cells/mouse, 5 mice/group) were subcutaneously injected into the axillary tissue by using a 27-gauge syringe. To establish the lung metastasis model in another 10 mice, negative control or HCC-LM3 cells with stable ZFPM2-AS1 knockdown (0.2 ml; $1x10^6$ cells/mouse, 5 mice/group) were intravenously injected into the tail vein of nude mice by using a 28-gauge syringe. The tumor volume (mm^3) in each mouse was measured by a Vernier caliper every 3 days and calculated as follows: Tumor volume=tumor length x $width^2/2$. Mice were euthanized following 21 days for the xenograft study and 50 days for the lung metastasis experiment. The following humane endpoints were established: Tumor diameter >2.0 cm, weight loss >25% and poor overall condition. None of the mice reached the humane endpoints in this study. To reduce suffering, mice were anesthetized with 2% isoflurane. Mice were then rapidly euthanized by cervical dislocation. Verification of death included cardiac and respiratory arrest, lack of reflection and changes in mucosal color. After subcutaneous tumors were dissected, tumors were weighed using a digital balance (Mettler), fixed with 4% formalin (Biosharp) and embedded with paraffin to prepare sections for histology. No metastatic nodules were found in the abdominal and thoracic organs of the subcutaneous xenograft mice. After death verification, lungs of the lung metastasis model mice were completely dissected. The lungs were fixed with 4% formalin (Biosharp), embedded in paraffin, cut into sections and stained with hematoxylin-eosin (H&E) for histopathological evaluation. Metastatic lung nodules were counted using a microscope (IX51; Olympus Corporation).

Chromosomal aberration assay. HCC cells with stable ZFPM2-AS1 knockdown were washed and treated with a demecolcine solution (cat. no. D1925; Sigma-Aldrich; Merck KGaA) for 2 h. The cells were collected and suspended in a hypotonic solution (0.075 M KCl) for 20 min at room temperature. The cells were then fixed in cold Carnoy's fixative (methanol/acetic acid, 3:1), placed on slides for staining with Giemsa (cat. no. G146-10; Thermo Fisher Scientific, Inc.) and examined by a microscope (DM2500; Leica Microsystems GmbH).

Nuclear and cytoplasmic RNA fractionation. Nuclear and cytoplasmic RNA was extracted using Nuclear and Cytoplasmic Extraction Reagents (Thermo Fisher Scientific, Inc.) following the manufacturer's protocol. RNA was subjected to RT-qPCR detection. GAPDH and U6 served as the cytoplasmic and nuclear controls, respectively.

RNA pull-down. The interaction between ZFPM2-AS1 and miR-3065-5p was validated using a Pierce Magnetic RNA-Protein Pull-Down Kit (Thermo Fisher Scientific, Inc.). The miR-3065-5p-WT (sequence: TCAACAAAATCACTG ATGCTGGA)/miR-3065-5p-MUT (sequence: TACGAG CGATCACTGATGCTGGA) and control were synthesized and biotin-labelled by Wuhan Jinkairui Bioengineering Co., Ltd. After being cultivated for 2 days, HCC cells were lysed. Cell lysates were then mixed with the biotinylated probes and

magnetic beads at 4°C for 1 h. RT-qPCR was used to verify the miR-3065-5p targets from the pull-down reaction mixture.

Immunohistochemistry (IHC). For IHC staining, 4 μm-thick slices of mouse tumor tissue were used. Paraffin sections were placed in an oven at 65°C for 2 h, dewaxed and washed three times with PBS (5 min each time). Primary antibody incubation was performed overnight at 4°C and secondary antibody incubation 50 min at 37°C. After labeling proteins, the staining was visualized using diaminobenzidine staining followed by hematoxylin counterstaining. Antibody information and dilution ratios are listed in Table SIV. After alcohol dehydration, a microscope (IX51; Olympus Corporation) was used to scan the slides at magnifications of x400 or x200. The mean optical density values of IHC images were determined using the IHC Toolbox plugin for ImageJ (v1.53e; NIH).

Luciferase reporter assay. A luciferase reporter assay was performed using the Dual-Luciferase Reporter Assay System (Promega Corp.) with the pmirGLO dual-luciferase miRNA target expression vector (Promega Corp.). HCC-LM3 cells were seeded in a 96-well plate and cultured overnight. They were cotransfected with miR-3065-5p mimics and ZFPM2-AS1 3'-untranslated region (UTR), XRCC4 3'-UTR, ZFPM2-AS1 3'-UTR-MUT or XRCC4 3'-UTR-MUT. Luciferase activities were measured using a dual-luciferase reporter gene assay system (Promega Corp.) and normalised to Renilla activity.

Cell proliferation, apoptosis, invasion and migration assays, Gene Ontology (GO), Kyoto Encyclopedia of Genes and Genomes (KEGG) enrichment analyses. The methods for these assays are provided in the supplementary methods S1.

Statistical analysis. All statistical analyses were performed using SPSS 25.0 software (IBM Corporation), GraphPad Prism 8.0 (GraphPad Software, Inc.) and R software (version 3.5.2). Categorical variables were compared using χ^2 tests. An unpaired Student's t-test was used to analyze two independent groups, while a paired t-test was used for paired samples. Multiple-group statistical comparisons were performed by one-way ANOVA with Tukey's multiple-comparisons test. Quantitation of the cell number, colony number, wound gap closure and WB band integrated density were performed with ImageJ software (v1.53e; NIH). Kaplan-Meier survival analysis was performed using the log-rank test. The Renyi test was performed to generate the P-values when survival curves crossed over. Cox proportional hazards models were applied to evaluate the hazard ratios (HR) in uni- and multivariate logistic regression analyses. All experiments were performed three times and P<0.05 was considered to indicate statistical significance.

Results

GI-linked lncRNAs are closely related to prognosis of patients with HCC. The processes performed in the present study are summarized in the flowchart in Fig. 1A. A total of 85 GI-linked lncRNAs with significant differences in expression between the high and low mutation groups were identified. Fig. S1 provides the results of various bioinformatics analyses. The expression levels of DNA damage-related proteins were closely associated with GI-linked lncRNAs. An lncRNA-mRNA coexpression network was then constructed (Fig. S1A) and genes coexpressed with these lncRNAs were significantly associated with GI according to GO and KEGG enrichment analyses (Figs. 1B and S1B). A total of 343 patients with HCC were randomly allocated into two groups: The training group (n=172) and the testing group (n=171). There were no significant differences between these groups in terms of any parameter (all P>0.05; Table SV). In the training group, 22 prognostic lncRNAs were screened out by univariate Cox regression analysis (Fig. S1C). In multivariate Cox regression analysis, only lung cancer-associated transcript 1 (LUCAT1), MIR210 host gene (MIR210HG) and ZFPM2-AS1 were significant (Fig. 1C). A GI-related lncRNA signature (GIlncsig) composed of six lncRNAs was established, with the

$$\text{GIlncsig} = \sum_{i=0}^{n} \text{coef}(\text{lncRNAi}) * \text{expr}(\text{lncRNAi})$$

following formula: (coef, coefficient of each lncRNA; expr, relative expression level of each lncRNA). The specific parameters are provided in Table SVI.

Validation of the predictive power of the model. The patients were divided into high-risk and low-risk groups based on the median risk score. The GIlncsig had a good clinical predictive performance in the training cohort (Fig. S2). In the testing cohort, the high-risk group had significantly worse outcomes than the low-risk group (P<0.001; Fig. 1D). The ROC curve analysis indicated good predictive power of the model [AUC=0.786; Fig. 1E]. The expression of DNA repair-related genes and somatic mutations were significantly higher in the high-risk group (P<0.05; Figs. 1F and S1D). Among the DNA repair-related genes, breast cancer gene 1 (BRCA1), RAD51 and XRCC4 were the most significant. The expression of prognosis-related lncRNAs differed significantly between the high- and low-risk groups (Fig. 1G) and the number of somatic mutations and DNA repair protein expression levels increased with increasing score (Fig. S1E). GIlncsig also exhibited a similar clinical predictive performance in the TCGA group (Fig. S3). Overall, multivariate Cox regression analysis in each group indicated GIlncsig to be a prognostic factor independent of other clinicopathological and mutational parameters (Table SVII). A Kaplan-Meier survival analysis indicated that the model was applicable to patients of different ages, pathological grades, genders and stages (Fig. S4). Significantly higher TP53 mutations were found in the high-risk group as compared with those in the low-risk group (P<0.01; Fig. 1H). The low-risk group with mutant TP53 had the best survival outcomes, whereas the high-risk group with wild-type TP53 had the worst survival outcomes (P=0.02; Fig. 1I). The model was then validated in the GEO datasets (GSE14520 and GSE76427) by using survival and ROC curve analyses (Fig. S5A-D).

ZFPM2-AS1 knockdown inhibits tumor development in vitro and in vivo. As ZFPM2-AS1 in GIlncsig had the largest HR value and the most significant P-value, ZFPM2-AS1 was selected for experimental research. the expression level of ZFPM2-AS1 was evaluated in 80 pairs of tissues (tumor tissues and corresponding adjacent nontumor tissues) and it was indicated to be highly expressed in tumor tissues (P<0.001; Fig. 2A). Kaplan-Meier analysis revealed
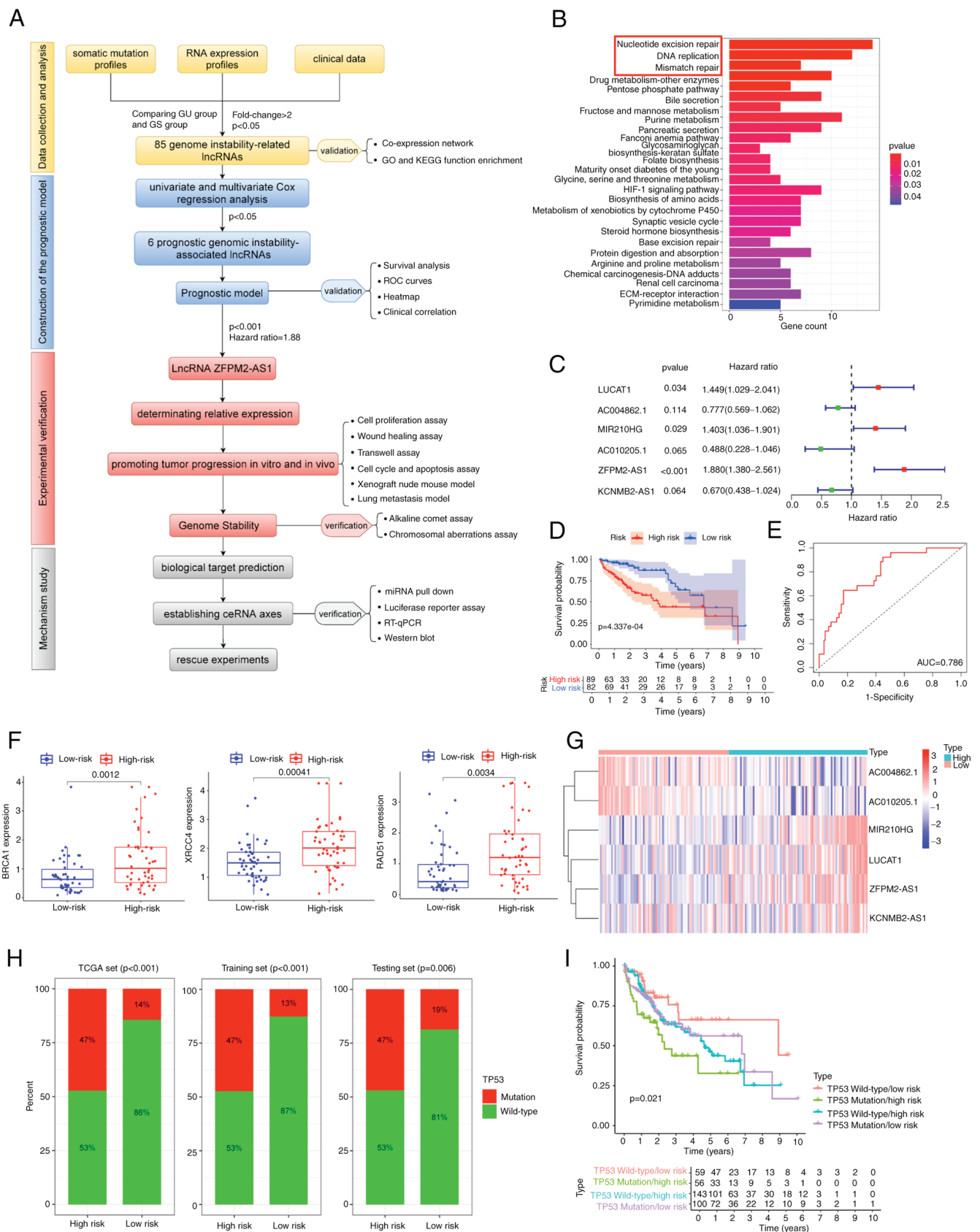
Figure 1. Development and verification of a genome instability-related lncRNA signature in hepatocellular carcinoma. (A) Flowchart of the study with cut-off values. (B) GO enrichment analysis for genes coexpressed with lncRNAs. (C) Forest plot with hazard ratios from multivariate Cox regression analyses. (D) Survival curve and (E) ROC curve analysis of GIlncsig in the testing group. (F) Comparison of the expression of three DNA repair proteins between different risk groups. (G) Heatmap illustrating the expression pattern of the six lncRNAs in GIlncsig with increasing risk score in the testing group. (H) Comparison of p53 mutation rates between the high- and low-risk groups. (I) Survival curves based on the combination of risk score and TP53 status. GO, Gene Ontology; KEGG, Kyoto Encyclopedia of Genes and Genomes; lncRNA, long noncoding RNA; TCGA, The Cancer Genome Atlas; ROC, receiver operating characteristic; AUC, area under the curve; RT-qPCR, reverse transcription-quantitative PCR; TP53, tumor protein 53; GIlncsig, genomic instability-related lncRNA signature.

Table I. Association of ZFPM2-AS1 expression with demographic and clinicopathological characteristics of patients with hepatocellular carcinoma (n=80).

| Characteristic | Cases, n (%) | ZFPM2-AS1 | | P-value |
		High	Low	
Age, years				0.370
<65	42 (52.5)	19	23	
≥65	38 (47.5)	21	17	
Gender				0.361
Female	32 (40.0)	18	14	
Male	48 (60.0)	22	26	
Tumor diameter, cm				0.014
<5	43 (53.8)	16	27	
≥5	37 (46.2)	24	13	
HBV infection				0.366
No	34 (42.5)	15	19	
Yes	46 (57.5)	25	21	
AFP, μg/l				0.369
<400	44 (55.0)	24	20	
≥400	36 (45.0)	16	20	
TNM				0.025
I+II	38 (47.5)	14	24	
III+IV	42 (52.5)	26	16	
Lymphatic invasion				0.044
No	43 (53.8)	17	26	
Yes	37 (46.2)	23	14	
PVTT				0.818
No	31 (38.8)	16	15	
Yes	49 (61.2)	24	25	

AFP, α-fetoprotein; PVTT, portal vein tumor thrombus; HBV, hepatitis B virus; ZFPM2-AS1, zinc finger protein, FOG family member 2 antisense 1.

that patients with high ZFPM2-AS1 expression had poor overall survival (P<0.001; Fig. 2B). ZFPM2-AS1 expression was associated with TNM stage, tumor size and lymphatic metastasis (P<0.05; Table I) according to the clinicopathological features of patients with HCC. Furthermore, it was indicated to be an independent prognostic factor (P=0.04; Table SVIII). The expression of ZFPM2-AS1 in the liver cancer cell lines was significantly higher than that in a normal liver cell line (Fig. 2C). It was indicated that shRNA#1 and shRNA#2 were able to significantly knock down ZFPM2-AS1 expression (P<0.001; Fig. 2D). ZFPM2-AS1 knockdown significantly inhibited the proliferation of HCC-LM3 and Huh7 cells (P<0.001; Fig. 2E and F) and impaired the invasion and migration of hepatoma cells (P<0.05; Fig. 2G-I). In an *in vivo* experiment, a subcutaneous tumor formation assay in nude mice indicated that ZFPM2-AS1 knockdown significantly inhibited tumor volume and tumor weight (P<0.05; Fig. 2J). Furthermore, no intrahepatic metastatic nodules were found according to H&E staining of mouse liver tissues (Fig. S5E). After RNA was extracted from the tumor tissue of the mice,

RT-qPCR revealed low expression levels of ZFPM2-AS1 in the ZFPM2-AS1 knockdown group (Fig. 2K). IHC of mouse tumor tissues suggested that Ki67 expression was decreased in the ZFPM2-AS1 knockdown group (Fig. 2L). In a separate experiment, ZFPM2-AS1 knockdown also reduced the formation of pulmonary metastatic nodules (Fig. 2M).

DNA damage increases after ZFPM2-AS1 knockdown. DNA damage was assessed using the comet assay and it was indicated that DNA damage in HCC-LM3 cells increased after ZFPM2-AS1 knockdown (P<0.05; Fig. 3A). Furthermore, ZFPM2-AS1 knockdown increased the number of chromosomal aberrations (Fig. 3B). DNA damage has been reported to induce apoptosis and cell-cycle arrest (24,25). Thus, the effect of ZFPM2-AS1 knockdown on cell apoptosis and the cell cycle was examined. Flow cytometric analyses suggested that knockdown of ZFPM2-AS1 promoted apoptosis and contributed to G1-phase arrest (Fig. 3C and D). Next, the expression of apoptosis- and cell cycle-related genes was examined. ZFPM2-AS1 knockdown significantly upregulated cleaved (CL) caspase 3 expression and
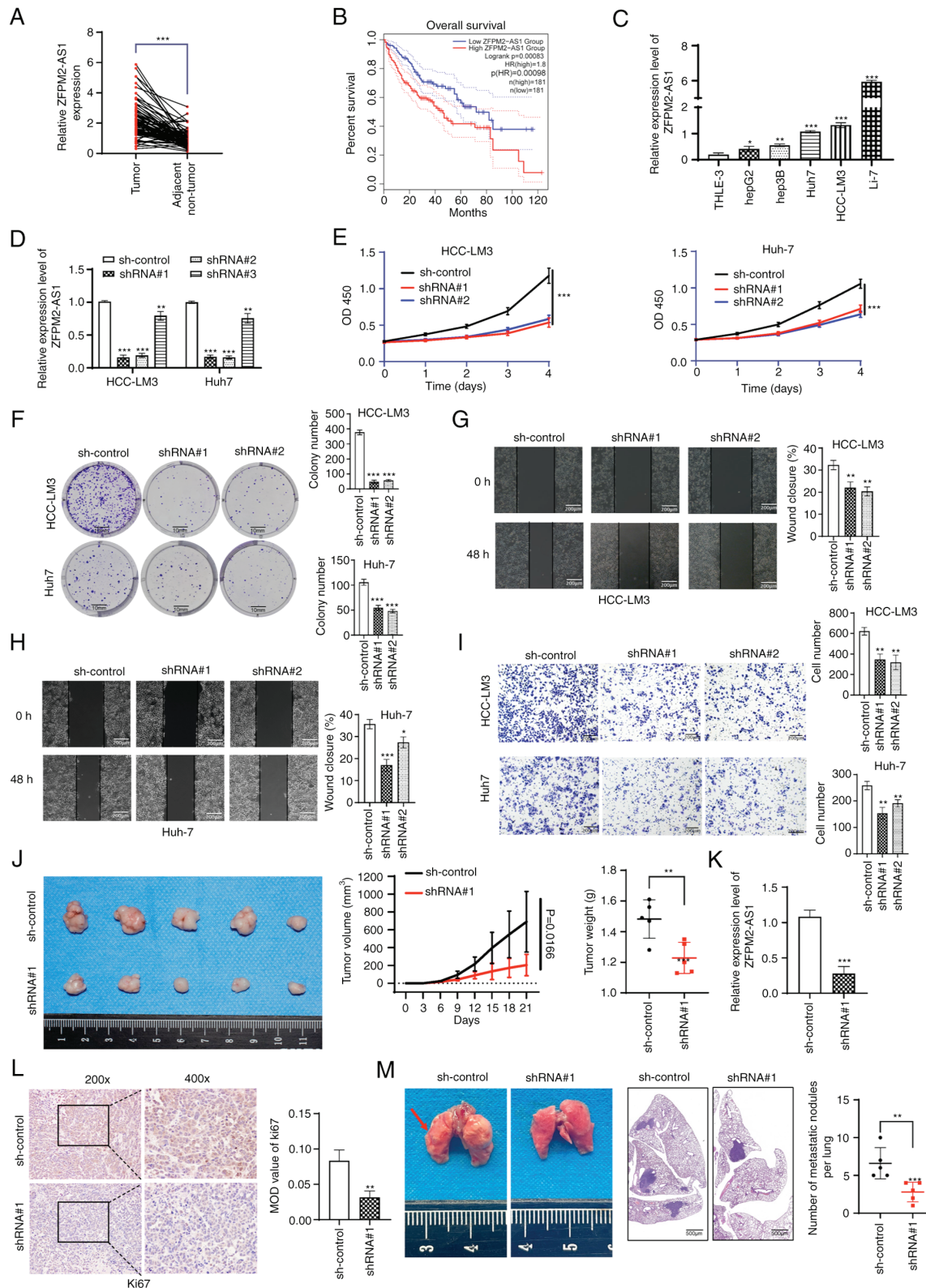
Figure 2. ZFPM2-AS1 knockdown inhibits hepatoma cell growth. (A) ZFPM2-AS1 expression was measured by quantitative PCR in 80 pairs of HCC and corresponding adjacent normal tissues. (B) Overall survival curves of patients with HCC based on GEPIA data. (C) Expression of ZFPM2-AS1 in five liver cancer cell lines and a normal liver cell line. (D) Knockdown efficiency of shRNA in HCC-LM3 and Huh-7 cells. (E and F) Cell proliferation was determined using (E) the Cell Counting Kit-8 assay and (F) a plate colony-formation assay (scale bars, 10 mm). (G and H) The migration ability of (G) HCC-LM3 and (H) Huh7 cells was detected using wound-healing experiments (scale bars, 200 μm). (I) Cell-invasion ability was detected using the Transwell assay (scale bars, 200 μm). (J) Volume and weight of subcutaneous xenograft tumors in nude mice. (K) ZFPM2-AS1 was significantly downregulated in subcutaneous xenograft tumors where ZFPM2-AS1-knockdown HCC-LM3 cells were injected. (L) IHC analysis of subcutaneous tumors showed that the expression level of Ki67 was reduced after ZFPM2-AS1 knockdown (magnification, x200 and x400). The MOD value was used for the quantification of IHC analysis. (M) ZFPM2-AS1 knockdown inhibited lung metastasis (scale bar in cm). The arrowhead indicates lung metastasis nodules. H&E staining results in lung tissue sections of each group (scale bar, 500 μm). The error bars and bars indicate the mean and standard deviation of at least three independent experiments. *P<0.05; **P<0.01; ***P<0.001. HCC, hepatocellular carcinoma; HR, hazard ratio; OD450, optical density at 450 nm; MOD, mean optical density; shRNA, short hairpin RNA; d, days; IHC, immunohistochemistry; ZFPM2-AS1, zinc finger protein, FOG family member 2 antisense 1; H&E, hematoxylin-eosin.
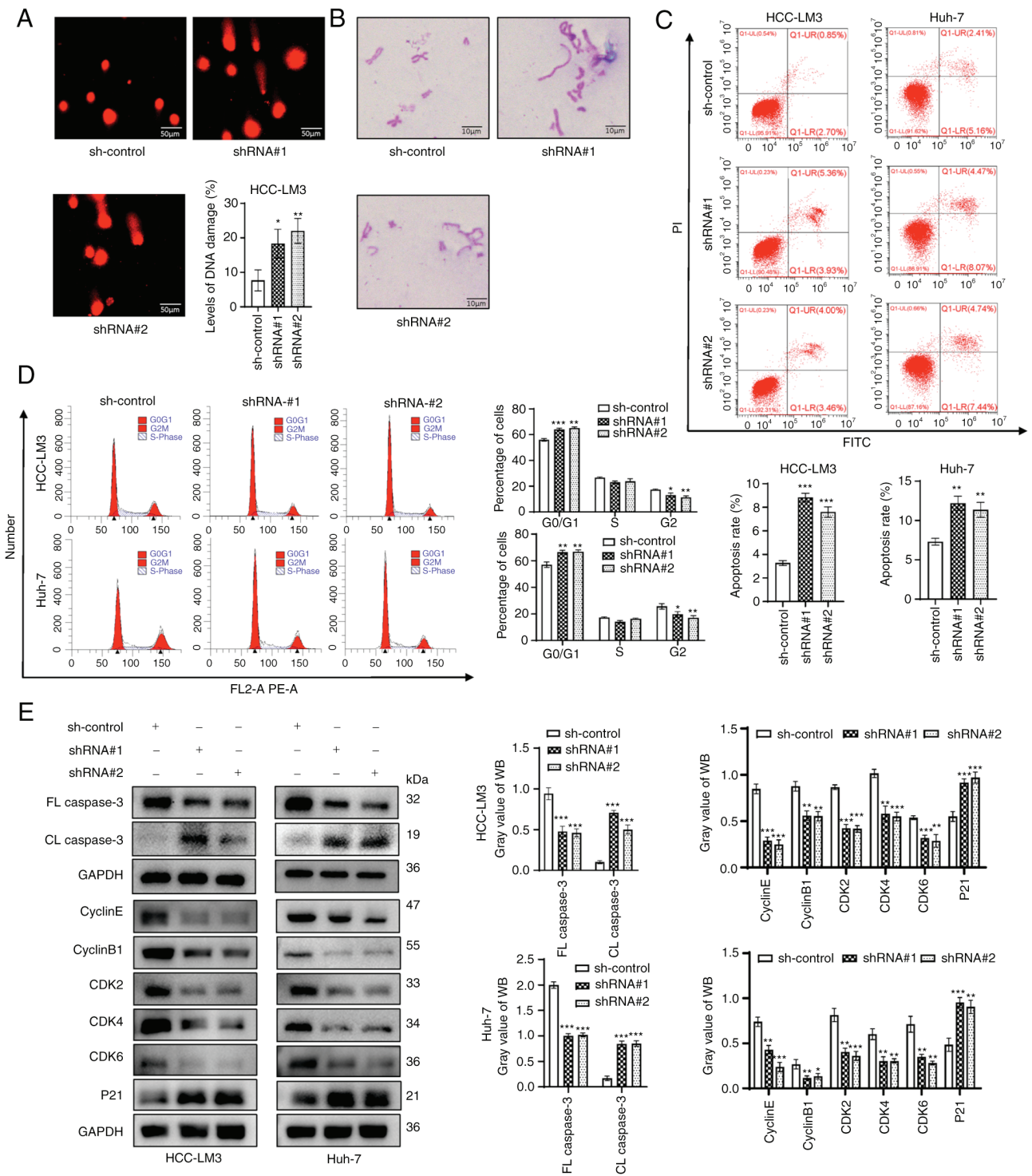
Figure 3. ZFPM2-AS1 knockdown induced DNA damage in hepatoma cells. (A) Level of DNA damage in HCC-LM3 cells (scale bar, 50 μm). (B) Distribution of chromosomal aberrations (scale bar, 10 μm). (C and D) Flow cytometry indicated that ZFPM2-AS1 knockdown (C) promoted apoptosis and (D) induced G1 arrest in hepatoma cells. (E) The effect of ZFPM2-AS1 knockdown on apoptosis and cell cycle progression was verified using WB assays. The error bars and bars indicate the mean and standard deviation of at least three independent experiments. *P<0.05; **P<0.01; ***P<0.001. FL, full length; CL, cleaved length; CDK, cyclin-dependent kinase; shRNA, short hairpin RNA; HCC, hepatocellular carcinoma; WB, western blot; PI, propidium iodide; ZFPM2-AS1, zinc finger protein, FOG family member 2 antisense 1.

downregulated full-length (FL) caspase 3 expression (apoptosis-related proteins). Furthermore, the expression of P21 was significantly upregulated, but that of cyclin E, cyclin B1, cyclin-dependent kinase 2 (CDK2), CDK4 and CDK6 (cell cycle-related proteins) was significantly downregulated after ZFPM2-AS1 knockdown (Fig. 3E).

ZFPM2-AS1 overexpression promotes hepatoma-cell growth and DNA repair. A plasmid was constructed to overexpress ZFPM2-AS1 in Hep3B cells, with the empty pcDNA3.1 vector used as a negative control. The overexpression efficiency of ZFPM2-AS1 was verified by RT-qPCR (Fig. 4A). It was confirmed that overexpression of ZFPM2-AS1 promoted the
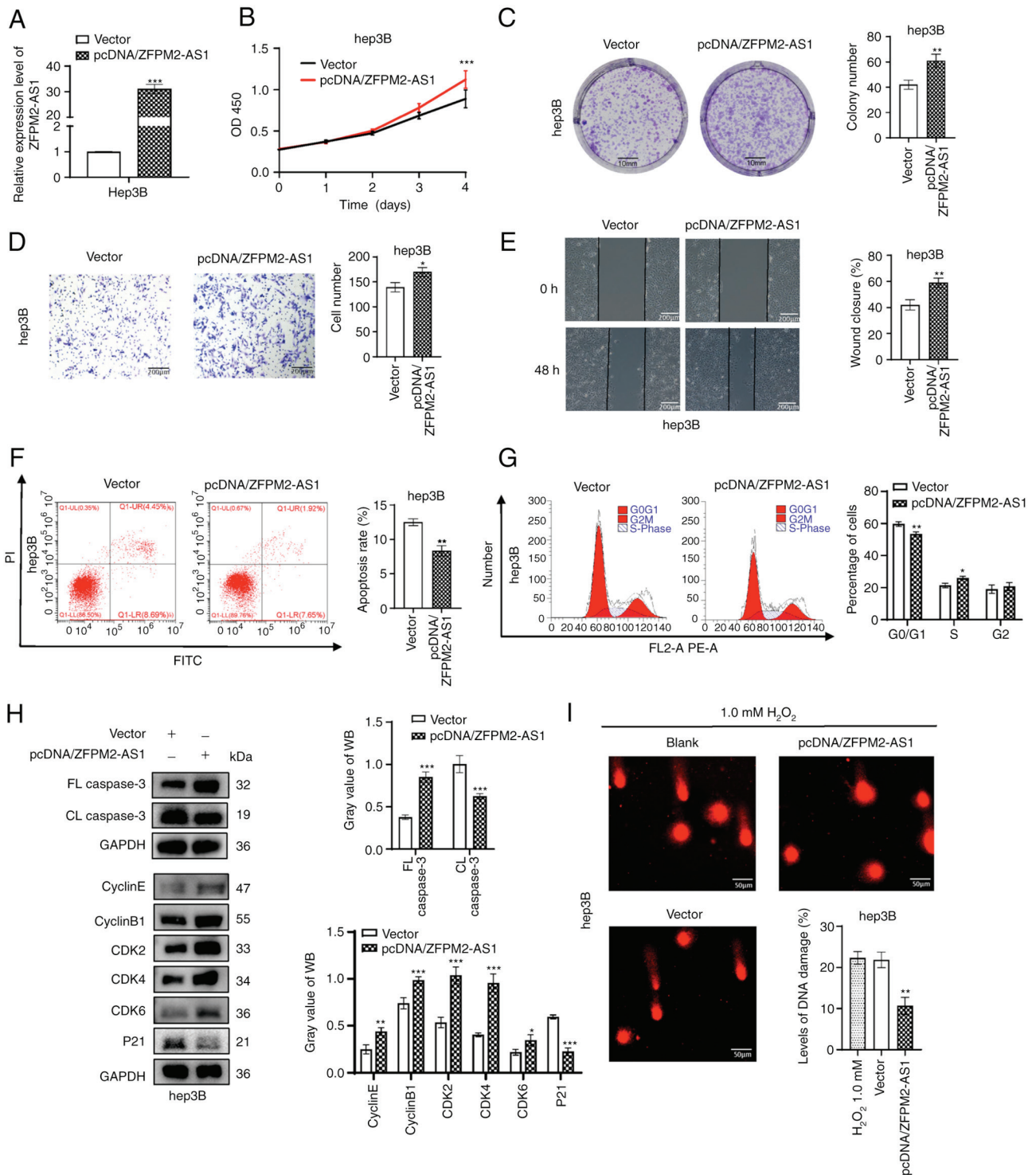
Figure 4. ZFPM2-AS1 overexpression promotes hepatoma cell progression. (A) Expression of ZFPM2-AS1 in Hep3B cells after transfection with pcDNA/ZFPM2-AS1. (B) Cell Counting Kit-8 and (C) plate colony formation assays (scale bars, 10 mm) indicated that ZFPM2-AS1 overexpression facilitated the proliferation of Hep3B cells. (D and E) Cell invasion and migration increased after ZFPM2-AS1 overexpression, as indicated by the (D) Transwell assay and (E) wound-healing assay, respectively (scale bars, 200 μm). (F) Apoptosis and (G) the cell cycle were assessed using flow cytometric analysis. (H) WB analyses revealed the expression of apoptosis- and cell cycle-related proteins. (I) An alkaline comet assay indicated that the DNA damage level was reduced after ZFPM2-AS1 overexpression in Hep3B cells. H_2O_2 (1.0 mM) was added to induce cell DNA damage (scale bars, 50 μm). The error bars and bars indicate the mean and standard deviation of at least three independent experiments. *$P<0.05$; **$P<0.01$; ***$P<0.001$. OD, optical density; d, days; FL, full length; CL, cleaved length; CDK, cyclin-dependent kinase; WB, western blot; PI, propidium iodide; ZFPM2-AS1, zinc finger protein, FOG family member 2 antisense 1.

proliferation, migration and invasion ability of hepatoma cells (Fig. 4B-E). Flow-cytometric analysis revealed that the apoptosis rate decreased and the S-phase population increased after pcDNA/ZFPM2-AS1 overexpression (Fig. 4F and G).

Similarly, WB results revealed that FL caspase3 was upregulated and CL caspase 3 was downregulated after ZFPM2-AS1 overexpression. In addition, ZFPM2-AS1 overexpression downregulated P21 and significantly upregulated cyclin E,
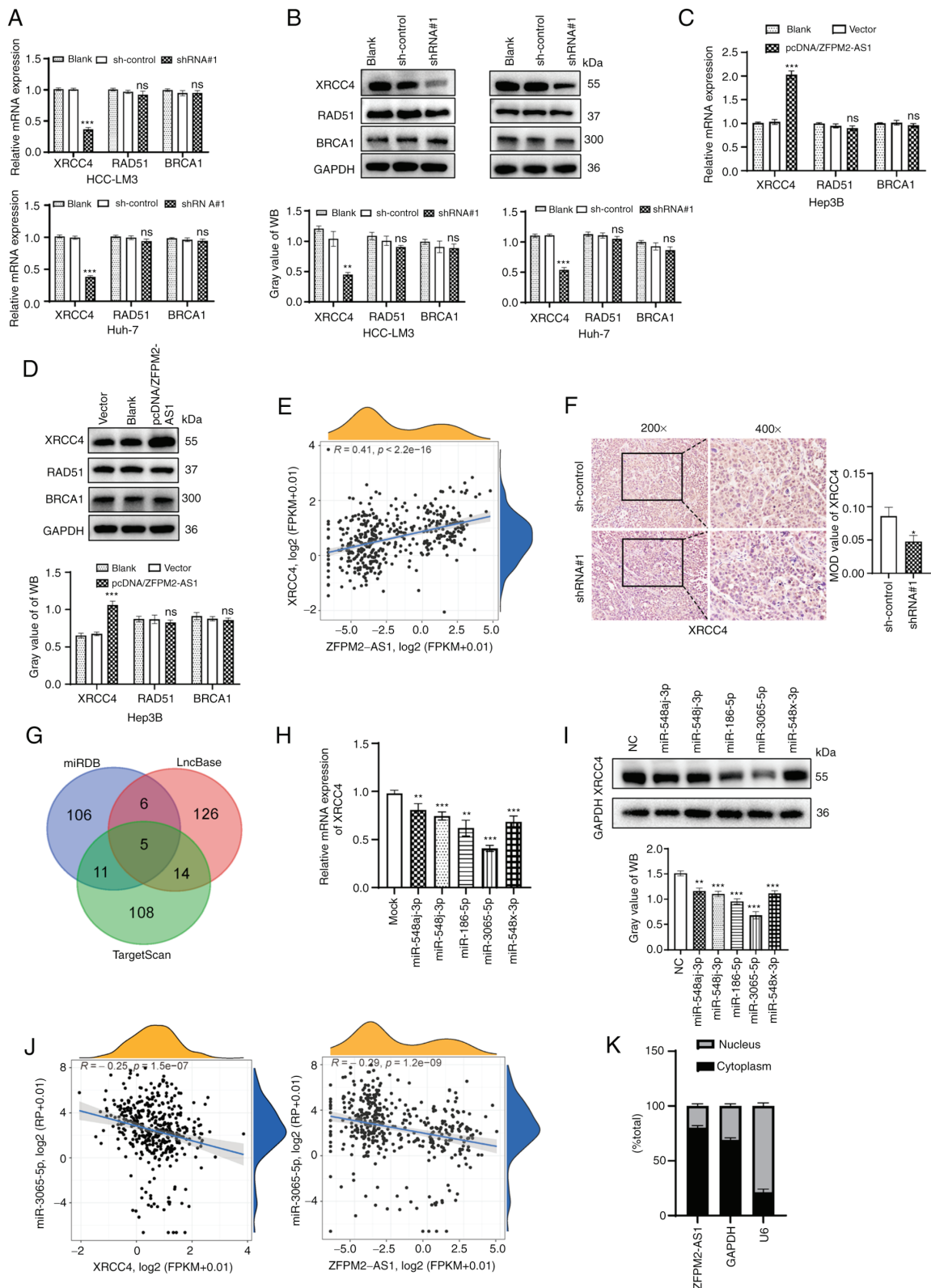
Figure 5. Expression of XRCC4 is affected by ZFPM2-AS1 and miR-3065-5p. (A and B) The expression levels of three DNA repair proteins after ZFPM2-AS1 knockdown in HCC-LM3 and Huh-7 cells were detected using (A) RT-qPCR and (B) WB assays. (C and D) Expression level of XRCC4 after ZFPM2-AS1 overexpression in Hep3B cells, as detected by (C) RT-qPCR and (D) WB. (E) Pearson correlation analysis was performed to evaluate the correlation between ZFPM2-AS1 and XRCC4 in the The Cancer Genome Atlas dataset. (F) XRCC4 was reduced after ZFPM2-AS1 knockdown, as indicated by IHC analysis (magnification, x200 and x400). Quantification of IHC analysis of XRCC4 expression. (G) Venn diagram indicating the predicted target miRNAs of ZFPM2-AS1 and XRCC4 from databases. (H) mRNA expression of XRCC4 after transfection of miRNA mimics in HCC-LM3 cells. (I) XRCC4 was significantly reduced by miR-3065-5p, as indicated by WB assay. (J) Pearson correlation analyses identified negative correlations between miR-3065-5p and XRCC4 or between miR-3065-5p and ZFPM2-AS1. (K) Nuclear and cytoplasmic RNA fractions were isolated from HCC-LM3 cells and analyzed by RT-qPCR. The error bars and bars indicate the mean and standard deviation of at least three independent experiments. *P<0.05; **P<0.01; ***P<0.001; ns, not significant. WB, western blot; RT-qPCR, reverse transcription-quantitative PCR; miR, microRNA; shRNA, short hairpin RNA; NC, negative control; IHC, immunohistochemistry; MOD, mean optical density; ZFPM2-AS1, zinc finger protein, FOG family member 2 antisense 1; RP, reads per kilobase per million mapped reads; XRCC4, X-ray repair cross complementing 4; BRCA1, breast cancer gene 1.
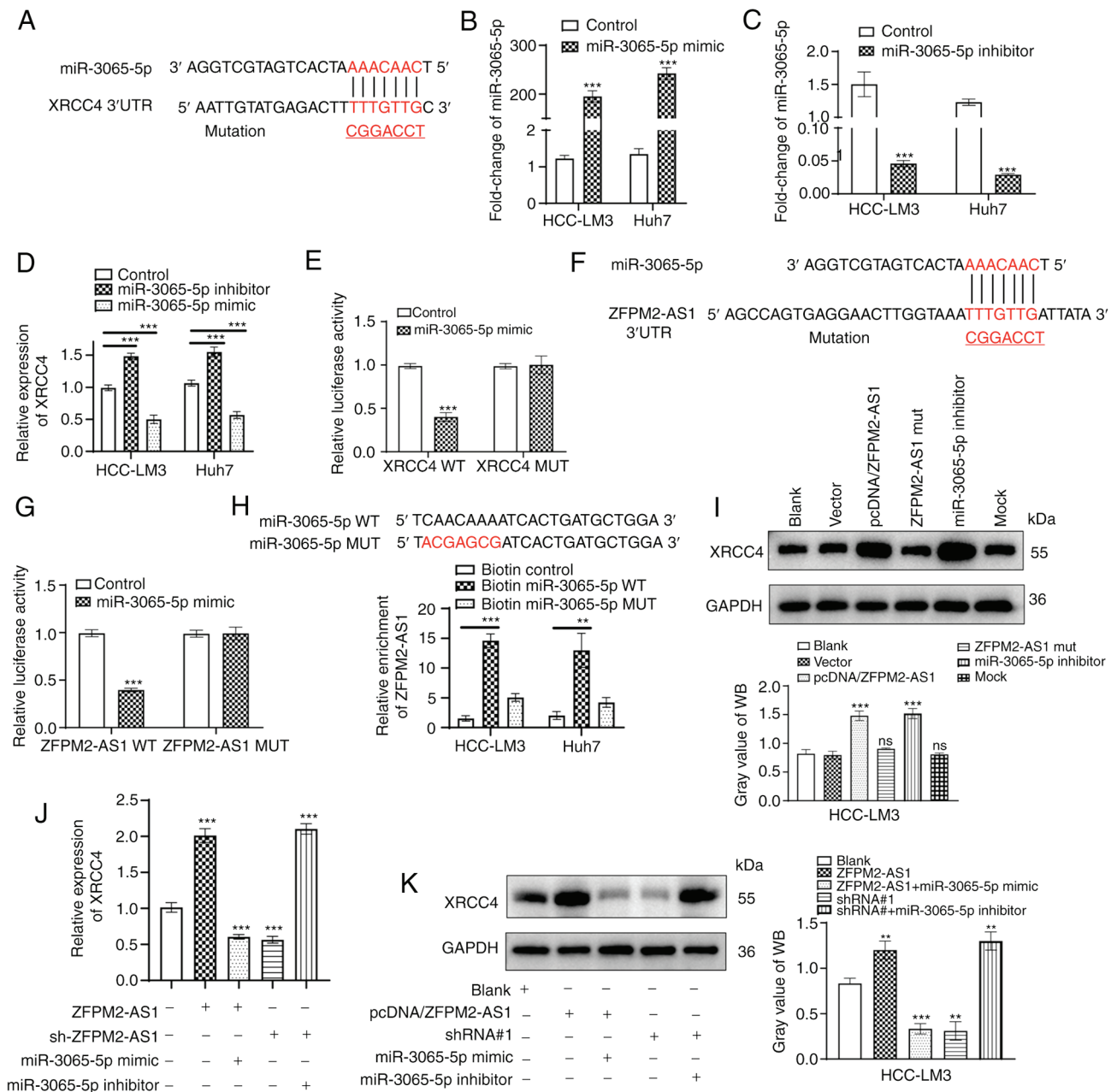
Figure 6. Mechanisms by which ZFPM2-AS1 regulates XRCC4. (A) Predicted binding sites for miR-3065-5p in the 3' UTR of XRCC4 and mutations in the binding sites are presented. (B and C) Expression levels of miR-3065-5p after transfection with (B) miR-3065-5p mimics and (C) inhibitor. (D) Effect of the miR-3065-5p mimics and inhibitor on XRCC4 expression. (E) Binding of miR-3065-5p and XRCC4 was examined using luciferase reporter assays. (F) Predicted binding sites for miR-3065-5p in the 3' UTR of ZFPM2-AS1 and mutations in the binding sites. (G) A luciferase reporter assay confirmed the direct interaction between miR-3065-5p and ZFPM2-AS1. (H) RNA pull-down indicated enrichment of ZFPM2-AS1 by application of biotin-labeled miR-3065-5p WT. (I) XRCC4 expression was upregulated by the miR-3065-5p inhibitor, as detected using WB assays. (J) RT-qPCR assay and (K) WB analysis indicated that the low expression level of XRCC4 was rescued after transfection with a miR-3065-5p inhibitor. The error bars and bars indicate the mean and standard deviation of at least three independent experiments. **$P < 0.01$; ***$P < 0.001$; ns, not significant. miR, microRNA; WB, western blot; RT-qPCR, reverse transcription-quantitative PCR; UTR, untranslated region; WT, wild-type; MUT, mutated; ZFPM2-AS1, zinc finger protein, FOG family member 2 antisense 1; XRCC4, X-ray repair cross complementing 4.

cyclin B1, CDK2, CDK4 and CDK6 (Fig. 4H). Cell DNA damage in the ZFPM2-AS1 overexpression group was significantly decreased compared with that in the control group, according to the comet assay ($P < 0.01$; Fig. 4I).

XRCC4 is influenced by ZFPM2-AS1 and miR-3065-5p. The GIlncsig indicated that XRCC4, BRCA1 and RAD51 were expressed at higher levels in the high-risk group compared to the low-risk group. Therefore, it was investigated whether

ZFPM2-AS1 influences the expression levels of these three proteins. After knockdown of ZFPM2-AS1 in HCC-LM3 and Huh-7 cells, XRCC4 was significantly downregulated. However, BRCA1 and RAD51 were not significantly altered (Fig. 5A and B). When ZFPM2-AS1 was overexpressed in Hep3B cells, the opposite result was observed ($P < 0.001$; Fig. 5C and D). ZFPM2-AS1 was positively correlated with XRCC4 in the TCGA dataset ($R = 0.41$, $P < 0.001$; Fig. 5E). IHC analysis revealed that ZFPM2-AS1 knockdown
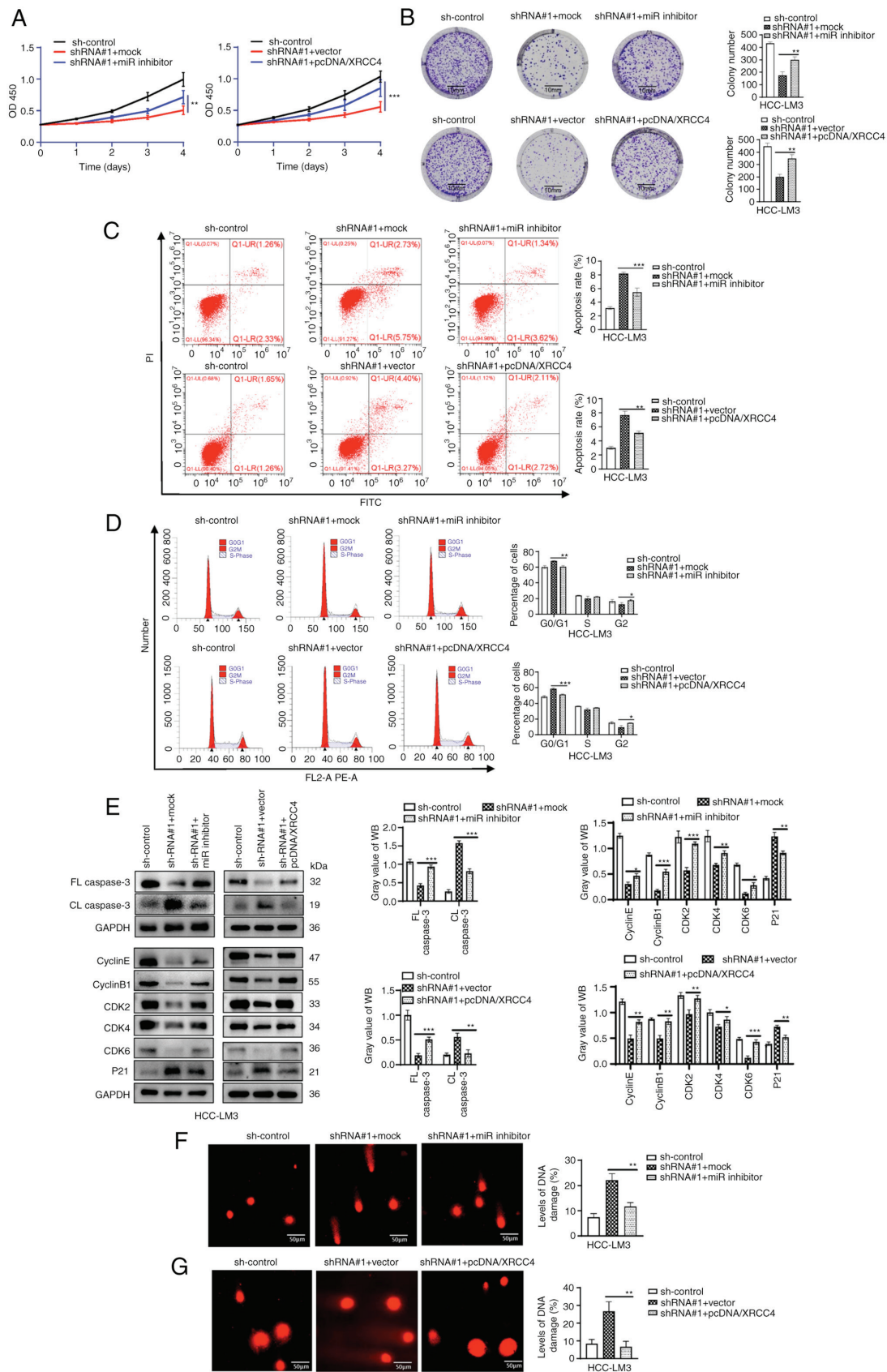
Figure 7. Zinc finger protein, FOG family member 2 antisense 1 facilitates hepatocellular carcinoma growth by regulating miR-3065-5p-mediated XRCC4. (A and B) Rescue experiments were conducted using sh-control, shRNA#1+mock, shRNA#1+miR inhibitor, shRNA#1+vector and shRNA#1+pcDNA/XRCC4 groups, with (A) Cell Counting Kit-8 and (B) colony-formation assays (scale bars, 10 mm). (C and D) miR-3065-5p inhibitor or pcDNA/XRCC4 rescued (C) the hepatoma cell cycle and (D) apoptosis as assessed by flow cytometry. (E) Apoptosis and cell cycle-related proteins were detected using WB assays. (F and G) The DNA damage level was rescued after transduction with (F) the miR-3065-5p inhibitor or (G) transfection with pcDNA/XRCC4 (scale bars, 50 μm). The error bars and bars indicate the mean and standard deviation of at least three independent experiments. *P<0.05; **P<0.01; ***P<0.001. OD, optical density; d, days; FL, full length; CL, cleaved length; CDK, cyclin-dependent kinase; WB, western blot; PI, propidium iodide; shRNA, short hairpin RNA; d, days; miR, microRNA; XRCC4, X-ray repair cross complementing 4.

downregulated XRCC4 expression in subcutaneous tumors (Fig. 5F). Since ZFPM2-AS1 altered XRCC4 at the mRNA and protein levels, it was hypothesised that ZFPM2-AS1 affected the transcriptional regulation of XRCC4 via a ceRNA mechanism. Subsequently, five candidate miRNAs (miR-548aj-3p, miR-548j-3p, miR-186-5p, miR-3065-5p and miR-548x-3p) were predicted in a screening for their ability to bind to ZFPM2-AS1 and XRCC4 by miRDB, LncBase and TargetScan (Fig. 5G). The mRNA expression of XRCC4 was significantly downregulated when hepatoma cells were transfected with miR-3065-5p mimics (P<0.001; Fig. 5H). This result was consistent with the WB results (P<0.001, Fig. 5I). In addition, a correlation analysis performed using the TCGA dataset revealed that miR-3065-5p expression was negatively correlated with XRCC4 and with ZFPM2-AS1 (R=-0.25 and -0.29, respectively, P<0.001; Fig. 5J). Nuclear and cytoplasmic RNA fractionation assays indicated that ZFPM2-AS1 was primarily expressed in the tumor cell cytoplasm (Fig. 5K).

ZFPM2-AS1 regulates XRCC4 by sponging miR-3065-5p. To further verify the present hypothesis, binding sites for miR-3065-5p and XRCC4 were predicted through the TargetScan database, and XRCC4 mutant plasmids were designed and synthesized (Fig. 6A). Furthermore, miR-3065-5p mimics and inhibitor were constructed, which had good transfection efficiency and significantly regulated mRNA expression levels of XRCC4 in hepatoma cells (Fig. 6B-D). A luciferase reporter assay revealed the interaction between miR-3065-5p and XRCC4, while no significant binding between miR-3065-5p and the XRCC4 mutant was observed (Fig. 6E). Similarly, the binding site between miR-3065-5p and ZFPM2-AS1 was predicted and ZFPM2-AS1 mutant plasmids were constructed (Fig. 6F). A luciferase reporter assay demonstrated the direct interaction between miR-3065-5p and ZFPM2-AS1, while miR-3065-5p did not significantly bind to the ZFPM2-AS1 mutant sequence (Fig. 6G). An RNA pull-down assay confirmed that ZFPM2-AS1 was significantly enriched by biotinylated miR-3065-5p WT (Fig. 6H). The ZFPM2-AS1 mutant had no effect on XRCC4, but the miR-3065-5p inhibitor markedly upregulated XRCC4 at the protein expression level (Fig. 6I). Through RT-qPCR and WB assays, it was verified that ZFPM2-AS1 regulated XRCC4 expression via miR-3065-5p (Fig. 6J and K). Overall, ZFPM2-AS1 acted as a ceRNA to regulate XRCC4 by binding to miR-3065-5p.

ZFPM2-AS1 regulates XRCC4 to accelerate HCC progression by competitively binding to miR-3065-5p. To demonstrate that ZFPM2-AS1 promotes HCC by regulating miR-3065-5p/XRCC4 axis, rescue experiments were performed (Figs. S6 and 7). The overexpression efficiency of pcDNA/XRCC4 was examined in HCC-LM3 cells by RT-qPCR and WB (Fig. S6A). According to CCK-8 and plate colony-formation assays, the cell proliferation ability was markedly decreased after ZFPM2-AS1 knockdown. However, when co-transducing with miR-3065-5p inhibitor or co-transfecting with pcDNA/XRCC4, the cell proliferation ability recovered noticeably again (Fig. 7A and B). In parallel, the miR-3065-5p inhibitor or pcDNA/XRCC4 reversed the high apoptosis rate and G1-phase arrest caused by ZFPM2-AS1

knockdown (Fig. 7C and D). The cell apoptosis and cycle-related protein expression detected by WB assay further validated the above conclusions (Fig. 7E). The Transwell and wound-healing assays demonstrated that the miR-3065-5p inhibitor or pcDNA/XRCC4 restored the inhibition of cell migration and invasion ability caused by ZFPM2-AS1 knockdown (Fig. S6B-D). In addition, the promoting effects of ZFPM2-AS1 knockdown on cell DNA damage were reversed by transduction with miR-3065-5p inhibitor or transfection with pcDNA/XRCC4 (Fig. 7F and G).

Discussion

Cancer develops from the clonal proliferation of a single aberrant cell (26). The cell frequently undergoes irreversible gene mutation and obtains functions that drive transformation into cancer. Mutations result from replication errors or DNA damage that is improperly repaired (27). Therefore, an abnormal DNA damage repair pathway is closely related to cancer progression.

An in-depth study of lncRNAs suggests that they have a significant role in cancer development (28,29). They lack the ability to encode proteins, yet have regulatory functions. LncRNA ENO1 intronic transcript 1 contributes to cancer growth by promoting glycolysis (30). Through the stabilization of PD-L1 protein and the degradation of GATA3 protein, lncRNA GATA3-AS1 promotes tumor immune evasion (31). Pivotal lncRNAs function as hinges between tumor metabolism and immunology (32). However, only a small number of studies have investigated lncRNAs related to GS. Therefore, the present study was performed and 85 GI-associated lncRNAs were identified. To examine the potential value of GI-related lncRNAs, a model composed of six lncRNAs was developed by Cox regression analysis. The model was then verified and a favorable prediction efficiency analysis was performed. The expression of DNA repair-related genes was significantly higher in the high-risk group. Among the DNA repair-related genes, BRCA1, RAD51 and XRCC4 were the most significant. The XRCC4, BRCA1 and RAD51 proteins promote DNA repair (33-36) and have an important role in maintaining genomic stability (37). Of note, the model still had excellent prognostic ability in the GEO validation groups. Therefore, the prognostic model is expected to be adopted by physicians in clinical applications. A significant proportion of patients with HCC with TP53 mutations have poor prognosis (38,39). The combination of GIlncsig and TP53 mutation status will provide a more accurate prognostic indicator for the diagnosis and treatment of HCC patients.

Among the six lncRNAs of the GIlncsig, the literature reports that LUCAT1, ZFPM2-AS1 and MIR210HG promote the progression of HCC (40-42). The biological functions of AC004862.1 and AC010205.1 have not been reported and potassium calcium-activated channel subfamily M regulatory β subunit 2 antisense 1 has not been reported in HCC. None of the six lncRNAs have been reported to affect GS. In the present study, ZFPM2-AS1 was selected as the focus of subsequent analyses, as it had the largest coefficient in the GIlncsig and the largest hazard ratio.

In the present study, ZFPM2-AS1 was indicated to be significantly upregulated in tumor tissues. ZFPM2-AS1
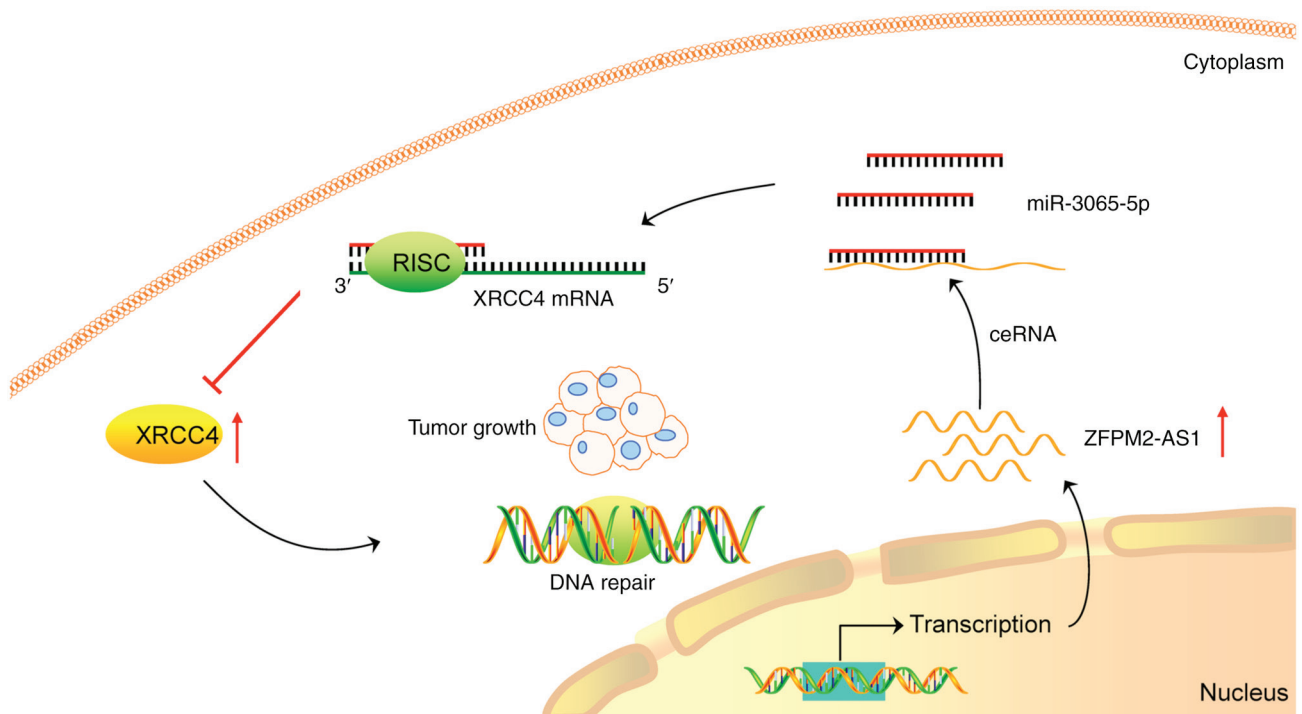
Figure 8. Mechanistic map depicting the role of the ZFPM2-AS1/miR-3065-5p/XRCC4 axis in the progression of HCC. ZFPM2-AS1 acted as a ceRNA by binding to miR-3065-5p. miR-3065-5p was loaded into the RISC and guided this complex to the 3' UTR of XRCC4 mRNA, leading to suppressed XRCC4 protein expression. Consequently, ZFPM2-AS1 upregulated XRCC4 by sponging miR-3065-5p to promote genomic stability and HCC progression. miR, microRNA; RISC, RNA-induced silencing complex; ceRNA, competing endogenous RNA; UTR, untranslated region; HCC, hepatocellular carcinoma; ZFPM2-AS1, zinc finger protein, FOG family member 2 antisense 1; XRCC4, X-ray repair cross complementing 4.

was demonstrated to increase the proliferation, migration and invasion ability of hepatoma cells *in vitro* and *in vivo*. The effects of ZFPM2-AS1 on apoptosis and cell-cycle progression were also verified using WB assays. Of note, the present study was the first to indicate that ZFPM2-AS1 knockdown increased DNA damage and chromosome aberrations in hepatoma cells. CeRNA is an important regulatory mechanism of lncRNAs (43). LncRNAs may serve as sponges for miRNAs through identical binding sites and modulate the function of miRNAs on their target mRNAs (44-46). The present study proved that ZFPM2-AS1 functions as a ceRNA to influence miR-3065-5p activity and regulates XRCC4. XRCC4 is an NHEJ protein that is recruited to DNA damage sites to mediate double-strand break repair and cell survival (47,48). In addition, XRCC4 increases the malignancy of breast cancer (49) but has not been reported in HCC, to the best of our knowledge. The present study discovered for the first time that miR-3065-5p is able to regulate DNA damage repair by mediating XRCC4. From the results of the luciferase reporter and RNA pull-down assays, it was indicated that miR-3065-5p directly interacted with ZFPM2-AS1 and XRCC4. Through rescue experiments, a new axis (ZFPM2-AS1/miR-3065-5p/XRCC4) in HCC was determined. This axis would be expected to be a key target for interfering with the progression of HCC in the future.

There are certain limitations to this study. Although the GIlncSig was applied to test its clinical predictive value in the TCGA and GEO samples, it requires further validation in a large cohort of tissue samples from clinical patients. It holds promise as a useful model in the prognosis prediction of patients with HCC. The other five lncRNAs in the GIlncsig were not validated in the initial experiments, and these lncRNAs will be validated in a follow-up study. Although ZFPM2-AS1 has been reported numerous times, its relationship with GS has not been previously reported, to the best of our knowledge. In the present study, ZFPM2-AS1 was analyzed because it was the most significant lncRNA in the current model. It was discovered that ZFPM2-AS1 had the ability to promote lung metastasis of HCC *in vivo*. In addition, an entirely novel ceRNA mechanism in HCC was investigated.

In conclusion, a prognostic model with excellent predictive performance for HCC was constructed. Through *in vivo* and *in vitro* functional experiments, it was verified that ZFPM2-AS1 promotes HCC progression and DNA damage repair. ZFPM2-AS1 was found to act as a ceRNA to promote GS and HCC proliferation via miR-3065-5p/XRCC4 (Fig. 8). During tumor progression, the genomic instability of tumors generally increases. However, the present results indicated that ZFPM2-AS1 facilitated DNA damage repair by upregulating XRCC4 to promote tumor progression, suggesting that GS may be a double-edged sword. The underlying mechanisms should be further investigated. The present study provides insight into the molecular mechanisms underlying GS and may offer a potential therapeutic strategy against HCC in the future.

Acknowledgements

Availability of data and materials

The datasets used and/or analyzed during the current study are available from the corresponding author on reasonable request.

Authors' contributions

HZ, ZL and JL designed experiments. HZ performed the bioinformatics analysis. JL, HZ, KX, YZ, and PX performed and analyzed the data. YZ assisted with the western blot analysis and methodology. KX concentrated primarily on the cell screening. JL, HZ and PX wrote the manuscript. JL was a major contributor in writing the manuscript. HZ, ZL and YY supervised the research. ZL and YY revised the manuscript critically for important intellectual content. YY provided the study's facilities. ZL and YY applied for the funding. JL and HZ confirmed the authenticity of all the raw data. ZL and YY agreed to be accountable for all aspects of the work. All authors have read and approved the final version of the manuscript.

Ethics approval and consent to participate

This study conformed to the Declaration of Helsinki. The tissue samples were collected with the approval of the ethics committee of Zhongnan Hospital (Wuhan, China; no. KELUN2020100). All of the patients provided written informed consent. All animal experiments were performed according to ethical guidelines and were approved by the ethics committee of Zhongnan Hospital (Wuhan, China; no. ZN2022006).

Patient consent for publication

Not applicable.

Competing interests

The authors declare that they have no competing interests.

References

1. Bray F, Ferlay J, Soerjomataram I, Siegel RL, Torre LA and Jemal A: Global cancer statistics 2018: GLOBOCAN estimates of incidence and mortality worldwide for 36 cancers in 185 countries. CA Cancer J Clin 68: 394-424, 2018.
2. Calderaro J, Couchy G, Imbeaud S, Amaddeo G, Letouzé E, Blanc JF, Laurent C, Hajji Y, Azoulay D, Bioulac-Sage P, et al: Histological subtypes of hepatocellular carcinoma are related to gene mutations and molecular tumour classification. J Hepatol 67: 727-738, 2017.
3. Ruiz de Galarreta M, Bresnahan E, Molina-Sánchez P, Lindblad KE, Maier B, Sia D, Puigvehi M, Miguela V, Casanova-Acebes M, Dhainaut M, et al: β-Catenin activation promotes immune escape and resistance to Anti-PD-1 therapy in hepatocellular carcinoma. Cancer Discov 9: 1124-1141, 2019.
4. Chaudhary R and Lal A: Long noncoding RNAs in the p53 network. Wiley Interdiscip Rev RNA 8: 10.1002/wrna.1410, 2017.
5. Feng J, Yang G, Liu Y, Gao Y, Zhao M, Bu Y, Yuan H, Yuan Y, Yun H, Sun M, et al: LncRNA PCNAP1 modulates hepatitis B virus replication and enhances tumor growth of liver cancer. Theranostics 9: 5227-5245, 2019.
6. Wang H, Ma P, Liu P, Guo D, Liu Z and Zhang Z: lncRNA SNHG6 promotes hepatocellular carcinoma progression by interacting with HNRNPL/PTBP1 to facilitate SETD7/LZTFL1 mRNA destabilization. Cancer Lett 520: 121-131, 2021.
7. Ishibashi M, Kogo R, Shibata K, Sawada G, Takahashi Y, Kurashige J, Akiyoshi S, Sasaki S, Iwaya T, Sudo T, et al: Clinical significance of the expression of long non-coding RNA HOTAIR in primary hepatocellular carcinoma. Oncol Rep 29: 946-950, 2013.
8. Wang C, Li Y, Yan S, Wang H, Shao X, Xiao M, Yang B, Qin G, Kong R, Chen R and Zhang N: Interactome analysis reveals that lncRNA HULC promotes aerobic glycolysis through LDHA and PKM2. Nat Commun 11: 3162, 2020.
9. Vishnubalaji R, Shaath H, Elango R and Alajez NM: Noncoding RNAs as potential mediators of resistance to cancer immunotherapy. Semin Cancer Biol 65: 65-79, 2020.
10. Tay Y, Rinn J and Pandolfi PP: The multilayered complexity of ceRNA crosstalk and competition. Nature 505: 344-352, 2014.
11. Lin X, Zhuang S, Chen X, Du J, Zhong L, Ding J, Wang L, Yi J, Hu G, Tang G, et al: lncRNA ITGB8-AS1 functions as a ceRNA to promote colorectal cancer growth and migration through integrin-mediated focal adhesion signaling. Mol Ther 30: 688-702, 2022.
12. Jeggo PA, Pearl LH and Carr AM: DNA repair, genome stability and cancer: A historical perspective. Nat Rev Cancer 16: 35-42, 2016.
13. Moynahan ME and Jasin M: Mitotic homologous recombination maintains genomic stability and suppresses tumorigenesis. Nat Rev Mol Cell Biol 11: 196-207, 2010.
14. Wickramasinghe VO and Venkitaraman AR: RNA processing and genome stability: Cause and consequence. Mol Cell 61: 496-505, 2016.
15. Shen L, Wang Q, Liu R, Chen Z, Zhang X, Zhou P and Wang Z: LncRNA lnc-RI regulates homologous recombination repair of DNA double-strand breaks by stabilizing RAD51 mRNA as a competitive endogenous RNA. Nucleic Acids Res 46: 717-729, 2018.
16. Munschauer M, Nguyen CT, Sirokman K, Hartigan CR, Hogstrom L, Engreitz JM, Ulirsch JC, Fulco CP, Subramanian V, Chen J, et al: The NORAD lncRNA assembles a topoisomerase complex critical for genome stability. Nature 561: 132-136, 2018.
17. Lee S, Kopp F, Chang TC, Sataluri A, Chen B, Sivakumar S, Yu H, Xie Y and Mendell JT: Noncoding RNA NORAD regulates genomic stability by sequestering PUMILIO Proteins. Cell 164: 69-80, 2016.
18. López EH and Palumbi SR: Somatic mutations and genome stability maintenance in clonal coral colonies. Mol Biol Evol 37: 828-838, 2020.
19. Roessler S, Jia HL, Budhu A, Forgues M, Ye QH, Lee JS, Thorgeirsson SS, Sun Z, Tang ZY, Qin LX and Wang XW: A unique metastasis gene signature enables prediction of tumor relapse in early-stage hepatocellular carcinoma patients. Cancer Res 70: 10202-10212, 2010.
20. Grinchuk OV, Yenamandra SP, Iyer R, Singh M, Lee HK, Lim KH, Chow PK and Kuznetsov VA: Tumor-adjacent tissue co-expression profile analysis reveals pro-oncogenic ribosomal gene signature for prognosis of resectable hepatocellular carcinoma. Mol Oncol 12: 89-113, 2018.
21. Chen X, Ma W, Yao Y, Zhang Q, Li J, Wu X, Mei C, Jiang X, Chen Y, Wang G, et al: Serum deprivation-response protein induces apoptosis in hepatocellular carcinoma through ASK1-JNK/p38 MAPK pathways. Cell Death Dis 12: 425, 2021.
22. Livak KJ and Schmittgen TD: Analysis of relative gene expression data using real-time quantitative PCR and the 2(-Delta Delta C(T)) Method. Methods 25: 402-408, 2001.
23. Xia P, Zhang H, Xu K, Jiang X, Gao M, Wang G, Liu Y, Yao Y, Chen X, Ma W, et al: MYC-targeted WDR4 promotes proliferation, metastasis, and sorafenib resistance by inducing CCNB1 translation in hepatocellular carcinoma. Cell Death Dis 12: 691, 2021.

24. Cai J, Wang N, Lin G, Zhang H, Xie W, Zhang Y and Xu N: MBNL2 Regulates DNA damage response via stabilizing p21. Int J Mol Sci 22: 783, 2021.
25. Lord CJ and Ashworth A: The DNA damage response and cancer therapy. Nature 481: 287-294, 2012.
26. Martincorena I and Campbell PJ: Somatic mutation in cancer and normal cells. Science 349: 1483-1489, 2015.
27. Al Zouabi L and Bardin AJ: Stem cell DNA damage and genome mutation in the context of aging and cancer initiation. Cold Spring Harb Perspect Biol 12: a036210, 2020.
28. Elguindy MM and Mendell JT: NORAD-induced Pumilio phase separation is required for genome stability. Nature 595: 303-308, 2021.
29. Zhang Y, He Q, Hu Z, Feng Y, Fan L, Tang Z, Yuan J, Shan W, Li C, Hu X, *et al*: Long noncoding RNA LINP1 regulates repair of DNA double-strand breaks in triple-negative breast cancer. Nat Struct Mol Biol 23: 522-530, 2016.
30. Hong J, Guo F, Lu SY, Shen C, Ma D, Zhang X, Xie Y, Yan T, Yu T, Sun T, *et al*: F: Nucleatum targets lncRNA ENO1-IT1 to promote glycolysis and oncogenesis in colorectal cancer. Gut 70: 2123-2137, 2021.
31. Zhang M, Wang N, Song P, Fu Y, Ren Y, Li Z and Wang J: LncRNA GATA3-AS1 facilitates tumour progression and immune escape in triple-negative breast cancer through desta-bilization of GATA3 but stabilization of PD-L1. Cell Prolif 53: e12855, 2020.
32. Yang J, Liu F, Wang Y, Qu L and Lin A: LncRNAs in tumor metabolic reprogramming and immune microenvironment remodeling. Cancer Lett 543: 215798, 2022.
33. Chen S, Lee L, Naila T, Fishbain S, Wang A, Tomkinson AE, Lees-Miller SP and He Y: Structural basis of long-range to short-range synaptic transition in NHEJ. Nature 593: 294-298, 2021.
34. Hatchi E, Goehring L, Landini S, Skourti-Stathaki K, DeConti DK, Abderazzaq FO, Banerjee P, Demers TM, Wang YE, Quackenbush J and Livingston DM: BRCA1 and RNAi factors promote repair mediated by small RNAs and PALB2-RAD52. Nature 591: 665-670, 2021.
35. Feretzaki M, Pospisilova M, Valador Fernandes R, Lunardi T, Krejci L and Lingner J: RAD51-dependent recruitment of TERRA lncRNA to telomeres through R-loops. Nature 587: 303-308, 2020.
36. Kim S, Jin H, Seo HR, Lee HJ and Lee YS: Regulating BRCA1 protein stability by cathepsin S-mediated ubiquitin degradation. Cell Death Differ 26: 812-825, 2019.
37. Arnould C, Rocher V, Finoux AL, Clouaire T, Li K, Zhou F, Caron P, Mangeot PE, Ricci EP, Mourad R, *et al*: Loop extru-sion as a mechanism for formation of DNA damage repair foci. Nature 590: 660-665, 2021.
38. Hussain SP, Schwank J, Staib F, Wang XW and Harris CC: TP53 mutations and hepatocellular carcinoma: Insights into the etiology and pathogenesis of liver cancer. Oncogene 26: 2166-2176, 2007.
39. Woo HG, Wang XW, Budhu A, Kim YH, Kwon SM, Tang ZY, Sun Z, Harris CC and Thorgeirsson SS: Association of TP53 mutations with stem cell-like gene expression and survival of patients with hepatocellular carcinoma. Gastroenterology 140: 1063-1070, 2011.
40. Lou Y, Yu Y, Xu X, Zhou S, Shen H, Fan T, Wu D, Yin J and Li G: Long non-coding RNA LUCAT1 promotes tumourigenesis by inhibiting ANXA2 phosphorylation in hepatocellular carci-noma. J Cell Mol Med 23: 1873-1884, 2019.
41. He H, Wang Y, Ye P, Yi D, Cheng Y, Tang H, Zhu Z, Wang X and Jin S: Long noncoding RNA ZFPM2-AS1 acts as a miRNA sponge and promotes cell invasion through regulation of miR-139/GDF10 in hepatocellular carcinoma. J Exp Clin Cancer Res 39: 159, 2020.
42. Wang Y, Li W, Chen X, Li Y, Wen P and Xu F: MIR210HG predicts poor prognosis and functions as an oncogenic lncRNA in hepatocellular carcinoma. Biomed Pharmacother 111: 1297-1301, 2019.
43. Yoon JH, Abdelmohsen K and Gorospe M: Posttranscriptional gene regulation by long noncoding RNA. J Mol Biol 425: 3723-3730, 2013.
44. Chen S, Xie C and Hu X: lncRNA SNHG6 functions as a ceRNA to up-regulate c-Myc expression via sponging let-7c-5p in hepatocellular carcinoma. Biochem Biophys Res Commun 519: 901-908, 2019.
45. Liu XH, Sun M, Nie FQ, Ge YB, Zhang EB, Yin DD, Kong R, Xia R, Lu KH, Li JH, *et al*: Lnc RNA HOTAIR functions as a competing endogenous RNA to regulate HER2 expression by sponging miR-331-3p in gastric cancer. Mol Cancer 13: 92, 2014.
46. Zhao CC, Jiao Y, Zhang YY, Ning J, Zhang YR, Xu J, Wei W and Kang-Sheng G: Lnc SMAD5-AS1 as ceRNA inhibit proliferation of diffuse large B cell lymphoma via Wnt/β-catenin pathway by sponging miR-135b-5p to elevate expression of APC. Cell Death Dis 10: 252, 2019.
47. Ochi T, Blackford AN, Coates J, Jhujh S, Mehmood S, Tamura N, Travers J, Wu Q, Draviam VM, Robinson CV, *et al*: DNA repair. PAXX, a paralog of XRCC4 and XLF, interacts with Ku to promote DNA double-strand break repair. Science 347: 185-188, 2015.
48. Gao Y, Ferguson DO, Xie W, Manis JP, Sekiguchi J, Frank KM, Chaudhuri J, Horner J, DePinho RA and Alt FW: Interplay of p53 and DNA-repair protein XRCC4 in tumorigenesis, genomic stability and development. Nature 404: 897-900, 2000.
49. Wen Y, Dai G, Wang L, Fu K and Zuo S: Silencing of XRCC4 increases radiosensitivity of triple-negative breast cancer cells. Biosci Rep 39: BSR20180893, 2019.